Experimental investigation of the interplay between optical and plasma smoothing induced on a laser megajoule beamline

S. Depierreux,[1,*] D. Pesme,[2] R. Wrobel,[1] D. T. Michel,[3,1] P.-E. Masson-Laborde,[1,4] G. Riazuelo,[1,4] E. Alozy,[1] N. Borisenko,[5] A. Orekhov,[5] M. Casanova,[1] A. Casner,[1] M. Grech,[3] A. Heron,[2] S. Huller,[2] P. Loiseau,[1,4] C. Meyer,[6] P. Nicolaï,[7] C. Riconda,[8] V. Tikhonchuk,[7] and C. Labaune[3]

[1]*Commissariat à l'énergie atomique et aux énergies alternatives (CEA), Direction des Applications Militaires (DAM), Île-de-France (DIF), F-91297 Arpajon, France*

[2]*Centre de Physique Théorique, Centre national de la recherche scientifique (CNRS), Ecole Polytechnique, 91128 Palaiseau cedex, France*

[3]*Laboratoire pour l'utilisation des lasers intenses (LULI), Unité mixte de recherche (UMR) 7605 Centre national de la recherche scientifique (CNRS), Ecole Polytechnique, 91128 Palaiseau Cedex, France*

[4]*CEA, LMCE, Université Paris-Saclay, 91680 Bruyères-le-Châtel, France*

[5]*P. N. Lebedev Physical Institute, 53 Leninskii Prospect, Moscow 119991, Russia*

[6]*Commissariat à l'énergie atomique et aux énergies alternatives (CEA), Direction des Applications Militaires (DAM), Centre d'études scientifiques et techniques d'Aquitaine (CESTA), F-33114 Le Barp, France*

[7]*University of Bordeaux, Centre national de la recherche scientifique (CNRS), Commissariat à l'énergie atomique et aux énergies alternatives (CEA), Centre lasers intenses et applications (CELIA), F-33405 Talence Cedex, France*

[8]*Sorbonne Université, Laboratoire pour l'utilisation des lasers intenses (LULI), Centre national de la recherche scientifique (CNRS), Commissariat à l'énergie atomique et aux énergies alternatives (CEA), École Polytechnique, Institut Polytechnique de Paris, F-75255 Paris, France*

(Received 3 May 2022; accepted 2 August 2023; published 19 October 2023)

Past experiments [S. Depierreux *et al.*, Phys. Rev. Lett. **102**, 195005 (2009)] have exhibited the plasma-induced incoherence (PII) process and the reduced imprint in the multikilojoule regime when a thin low-density foam is disposed in front of a solid target. Complementary experiments have been designed to analyze the mechanisms involved, the important parameters, and the role of the optical smoothing in the case of the laser megajoule. Forward stimulated Brillouin scattering (FSBS) is identified as the dominant mechanism governing the angular spray of the laser. FSBS also increases the laser bandwidth and imparts levels of temporal and spatial incoherencies beyond the present capacities of the optical smoothing of the megajoule laser facilities. Such a PII beam becomes suitable to achieve the high degree of irradiation uniformity required to experiment high-convergence efficient direct-drive inertial confinement fusion configurations at the megajoule scale which would otherwise require major changes in the laser chains. By reducing backscattering losses and/or allowing less optically applied smoothing, PII could relax the constraints imposed on the laser system and open the road to an increase in the energy coupled to the target in indirect-drive experiments.

DOI: 10.1103/PhysRevResearch.5.043060

I. INTRODUCTION

High-energy megajoule laser facilities of interest for inertial confinement fusion (ICF) [1,2] (like the Laser Mégajoule (LMJ) and the National Ignition Facility (NIF)) make use of optical smoothing techniques to shape the on-target intensity distribution. Continuous phase plates (CPPs) [3] split the $f/20$ aperture of their beams into independent $\sim f/1000$ beamlets that yield millimeter focal spots over Rayleigh lengths >1 cm. The interference of these beamlets in the focal plan creates many diffraction-limited micrometer-sized structures, called speckles. A frequency modulation of the laser combined with diffraction gratings rapidly displaces these speckles [4]. This smooths the time-averaged irradiation of the target and its hydrodynamic response. The LMJ optical system is unique, as it exploits the same gratings [5] to focus the beams and provide the chromaticism needed for this temporal smoothing. Increasing the spectral bandwidth is also expected to continuously reduce the growth of the resonant laser-plasma instabilities [6–12]. Since increasing the level of applied optical incoherence comes at the expense of the reduction of the laser energy delivered on target and/or growing optical damage [13–17], one can take advantage of the additional incoherence induced on the beams as they propagate through the plasma in front of the target. This option in the case of megajoule facilities raises specific questions linked to the long focal lengths (8 m) and large focal volumes of their beamlines. In addition, since the plasma-induced incoherence

*sylvie.depierreux@cea.fr

(PII) may be less efficient on these incoherent laser beams, it also requires first understanding the interplay between their optical and plasma smoothing.

Several mechanisms coupling the laser electromagnetic wave with the transverse ion dynamics have been identified as responsible for PII: self-focusing (SF) [18], filament instability [19], forward stimulated Brillouin scattering (FSBS) [20], and multiple FSBSs [21,22]. SF could develop in individual speckles carrying an optical power P_{sp} larger than the critical power for SF $P_c(\mathrm{MW}) = 34\ T_e\,(\mathrm{keV})\frac{\sqrt{1-(n_e/n_c)}}{n_e/n_c}$ [23–25]. In a speckle characterized by $P_{sp}/P_c > 1$, SF is expected to dominate linear diffraction, leading to speckle contraction and ultimately to trapping light in density channels, thus creating filaments that may become unstable. The speckles diameter and their distribution of intensities in a CPP-smoothed megajoule facility beamline almost necessarily entail the presence of speckles with $P_{sp}/P_c > 1$ in the focal volume [26]. More than half the total beam power is in such speckles if $n_e/n_c > 0.12$ at $T_e \leqslant 2\,\mathrm{keV}$. FSBS is the resonant coupling of the laser wave with an ion-acoustic wave (IAW) to produce a scattered redshifted electromagnetic wave propagating forward at a small angle with respect to the laser beam direction. In contrast with SF taking place in the high-intensity speckles, FSBS develops as a collective instability [21,22,27–33], and the spatial gain of scattered wave amplitude depends on the full beam power. Since the amplitude of the scattered waves increases with the propagation distance, FSBS may repeat itself by inducing the secondary FSBS decays, thus broadening the frequency spectrum of the laser beam and its angular width. FSBS may play a significant role in smoothing the beams on megajoule facilities, where multiple FSBSs could substantially rise in millimeter-long low-density plasmas. A regime of coherent FSBS was suggested by Lushnikov *et al.* [28] (in the case with temporal smoothing) and by Grech *et al.* [30] (in the case without temporal smoothing and below the self-focusing threshold). Reference [30] proposed a criteria for beam spray corresponding to the growth of this coherent FSBS.

SF and/or FSBS have been the subject of many experimental studies [34–42], mainly based on transmitted light diagnostics [43]. Recent experiments [42] performed below the SF threshold found a good agreement with the criteria [30]. Care was taken on reproducing millimeter-long propagation distances, but the available laser energy has limited these studies to $\sim$100 μm spot size except for a few experiments [44,45]. In this paper, we report on unique experiments exploiting extensive diagnostics of the transmission of an LMJ beamline after its propagation through a low-Z [46] plasma relevant to ICF designs. A broad range of parameters involved in such designs [11,47,48] has been explored experimentally by varying the initial plasma densities and lengths with, in addition, time-resolved measurements enabling us to monitor the transmitted light as the plasma parameters evolve. Time and spectrally resolved data clearly identify FSBS as the dominant mechanism governing the beam angular spray. The presence of multiple FSBSs, previously inferred only from numerical simulations, is demonstrated from the measured increase of the transmitted light spectral bandwidth with the plasma length. Although the small LMJ beam aperture produces large speckles which are *a priori* prone to SF, FSBS is found to prevail and to inhibit SF. We show that the temporal smoothing technique specific to LMJ reduces FSBS but does not prevent its growth. A theoretical analysis is set forth for the FSBS of incoherent beams which properly accounts for the experimental observations.

II. METHODS

The experiment was carried out on the LIL facility representing one LMJ beamline made of four square beams of section $D = 0.4\,\mathrm{m}$ separated by $d = \sim 0.17\,\mathrm{m}$. This quadruplet was fired at a power 3.5 TW in 1.5, 2, and 2.7 ns square pulses. The final optics assembly of each individual beam comprises a grating at the main laser wavelength of 1.053 μm (1ω) followed by two KDP crystals that convert light to the wavelength $\lambda_0 = 0.351\,\mu\mathrm{m}\,(3\omega)$. Then a 3ω grating (focal length $f = 8\,\mathrm{m}$), placed after a CPP, focuses the beam. The four beams were superimposed and focused on target with an aperture $\Delta\theta_0 = \pm 3.5^\circ$ [$\sin(\Delta\theta_0) = (D + d/2)/f$] in a Gaussian spot. For these parameters, the speckle radius is 1.5 μm [22]. The intensity maximized at $I_{\max} = 2.1\times10^{15}\,\mathrm{W/cm^2}$ and averaged at $1\times10^{15}\,\mathrm{W/cm^2}$ in the 600-μm-diameter focal spot measured at $0.1 \times I_{\max}$. The chromaticism of focusing gratings creates a longitudinal temporal smoothing by spectral dispersion (LSSD) [5,49,50]. Two electro-optic modulators introduce spectral broadening in the laser source. The first one (2 GHz) is mandatory to avoid stimulated Brillouin scattering in the optics. The second one operates at 14 GHz (modulation depth 5). In the following, "with" and "without LSSD" refer to configurations with or without this modulator.

The targets were $C_{12}H_{16}O_8$ foams [51] of initial densities 3–7 mg/cc and lengths 300–1000 μm. The foam was encased in washers of diameter 2.5 mm, giving a wide-open geometry for the propagation of the laser and detection of the transmitted light. Figures 1(b) and 1(c) show the plasma parameters as computed by the two-dimensional Lagrangian code FCI2 (benchmarked [52] with experimental data). The main diagnostics [Fig. 1(a)] measured the time-resolved spectra and power of the light transmitted at multiple angles. A rapid photodiode gave the time evolution of the direct transmission. The light transmitted around the initial beam aperture impacted a plane diffuser imaged on a charge-coupled device camera for time-integrated measurements of its angular diagram. Four absolutely calibrated fast photodiodes were installed in transmission at each of the three angles (θ_s) : 12°, 20°, and 30°. Finally, the time-resolved spectra of the light scattered at 12° and 20° were measured with a 0.2 Å spectral resolution. The two signals were multiplexed on the same combination of a high-resolution spectrometer (focal length 1.25 m and 3600 g/mm gratings) with a S20 streak camera. The temporal resolution, similar for all time-resolved diagnostics, was 200 ps.

III. RESULTS AND DISCUSSION

We first consider the case of a 7 mg/cc, 500-μm-long foam. The laser pulse, the direct transmission, and the light scattered at 12° are shown in Figs. 2(a) and 2(b) as a function of time

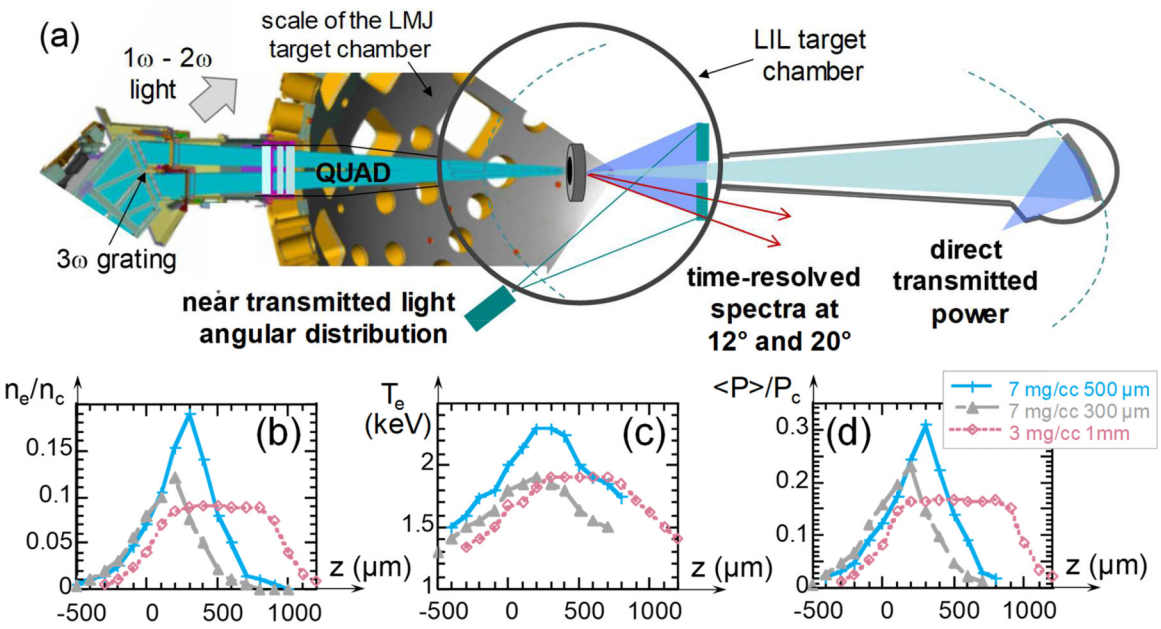

FIG. 1. (a) Sketch of the experimental setup. (b) Electron density and (c) temperature profiles computed at $t \sim 1.35$ ns for three different foams; the foam entrance plan is in $z = 0$; (d) corresponding $\langle P \rangle / P_c$, where $\langle P \rangle$ is the power computed in a speckle at 1.5×10^{15} W/cm^2.

with or without LSSD applied. The 2 ns laser pulse starts at $t = 0$ ns, rises until $t \sim 0.6$ ns, and the transmission starts at $t \sim 1$ ns. As expected from modeling [53] and observation of the ionization front in previous experiments [54–62], the laser and foam parameters resulted in the supersonic ionization of the low-density foam. The average ionization front velocity computed from the delay between the incident and transmitted pulses is $v = 8 \times 10^7$ cm/s, while the sound velocity is $C_s \sim 3 \times 10^7$ cm/s. For $t = 1$–2.2 ns, the direct transmitted light level increases due to the plasma expansion and subsequent decrease in collisional absorption.

At $t = 1$ ns, transmitted light was simultaneously observed at larger angles. The light scattered at 12° is shown as a function of time in Fig. 2(b). First notice that the time modulation at a 500 ps period (corresponding to the 2 GHz modulator), apparent in the laser power [Fig. 2(a)] especially in the shots without LSSD, is exacerbated in Fig. 2(b), as one can expect for a nonlinear effect. Otherwise, the light scattered at 12° stayed at an approximately constant level throughout its duration ~0.7 ns in contrast to the direct transmission that continuously increased. The images of the surrounding diffuser plate gave a more complete view of the angular distribution of the energy transmitted around the initial beam aperture and evidenced that the transmitted light exhibited a round shape after crossing the plasma [63,64]. The corresponding angular distribution, plot in Fig. 2(c), is approximately Lorentzian with a width ±8° (measured at half maximum) to be compared with the focusing aperture $\Delta\theta_0 = \pm 3.5°$. These results are processed to infer the total amount of energy scattered outside the initial aperture. In the shot performed with LSSD, one finds 330 J in the range $\theta_s = 4°$–$7°$, 200 J in the range $\theta_s = 7°$–$10°$, and 160 J with $\theta_s > 10°$. Based on Fig. 2(b), it is reasonable to assume that this latter energy was scattered for ~0.7 ns, thus giving a power ~0.23 TW scattered at $\theta_s > 10°$ for $t = 1$–1.7 ns. Thus, large amounts of the total transmitted power were scattered outside the initial beam aperture when the transmission started. LSSD reduced the amount of forward scattered light by a factor ~1.5 over the full angular range.

These results were complemented by similar data acquired for a 3 mg/cc-1000 μm foam without LSSD. Figure 2(a) shows that keeping the total amount of material nearly constant along the beam path resulted in a direct transmitted pulse close to that measured in the 7 mg/cc-500 μm foam.

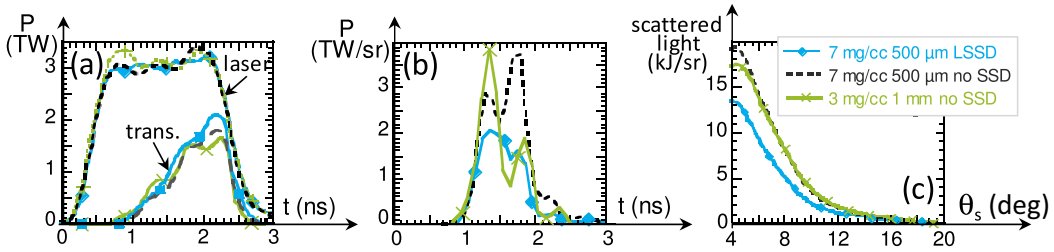

FIG. 2. (a) Laser pulse and power transmitted inside the original beam aperture for shots with and without longitudinal temporal smoothing by spectral dispersion (LSSD). (b) Corresponding power scattered at $\theta_s = 12°$. (c) Time-integrated angular distribution of the transmitted light.

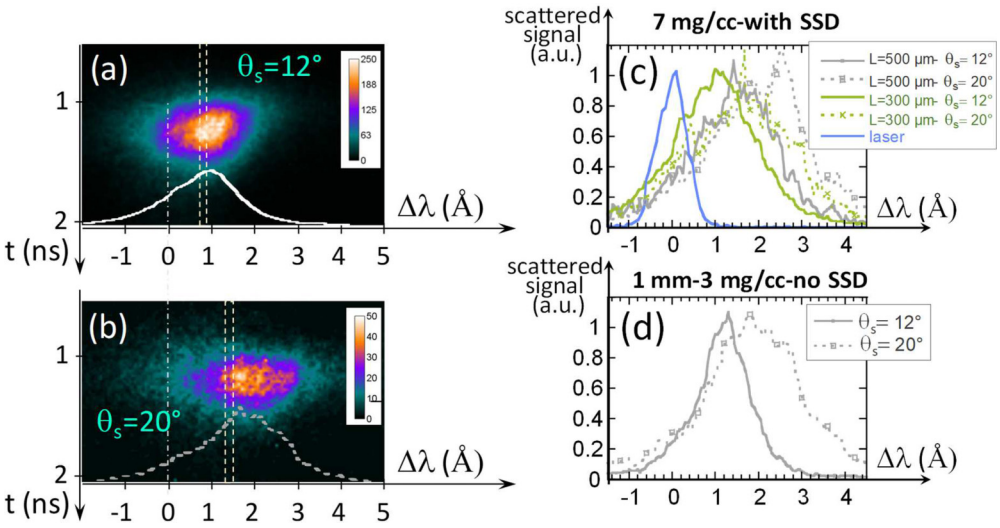

FIG. 3. Time-resolved spectra measured at (a) $\theta_s = 12°$ and (b) $\theta_s = 20°$ in a 7 mg/cc-300-μm-long foam with longitudinal temporal smoothing by spectral dispersion (LSSD). The dashed vertical lines delineate the expected wavelength range for single forward stimulated Brillouin scattering (FSBS) scattering. The trace of the time-integrated signal is superimposed on the spectrum measured at each angle. Spectra measured at the two angles integrated over 200 ps when the transmission just starts in shots performed (c) with LSSD and (d) without LSSD. The curve "laser" in (c) corresponds to the laser spectrum measured in vacuum when LSSD is applied.

A similar conclusion holds for the amount of light scattered at larger angles [see Figs. 2(b) and 2(c)]. This is surprising since the maximum value of $\langle P\rangle/P_c$ [Fig. 1(d)] ($\langle P\rangle/P_c > 0.25$) in the 7 mg/cc-500 μm foam and the distribution of speckles intensities for the CPP-smoothed beam imply that more than half the total beam power is in speckles for which $P_{sp}/P_c > 1$. In contrast, the value $\langle P\rangle/P_c (< 0.16)$ in the 3 mg/cc − 1000 μm foam plasma corresponds to <10% of the total beam power in speckles with $P_{sp}/P_c > 1$. Thus, the fact that the large angle scattering observed in the 3 mg/cc-1 mm foam is close to that in the 7 mg/cc-500 μm is strong evidence that SF barely contributed to the angular spray of the transmitted beam. This result invalidates standard criteria based on local $\langle P\rangle/P_c$ values to quantify beam spray in ICF experiments [40,41].

The effect of plasma length was investigated in the LSSD configuration through shots performed in 7 mg/cc foams (see Appendix A).

The mechanisms at play in the observed beam spraying were further investigated with time-resolved spectra measured at $\theta_s = 12°$ and 20°. These results are displayed in Figs. 3(a) and 3(b) in the case of a 7 mg/cc-300 μm foam with LSSD applied. The scattered light is redshifted with a mean spectral shift increasing with θ_s, as one would expect from FSBS. The mean spectral shift measured at 12° decreases as a function of time from ∼1 Å (at $t = 1$ ns) to 0.75 Å (at $t = 1.4$ ns), this latter value being the expected one for a single FSBS step. At each scattering angle, the spectral broadening ∼1.5 Å measured in this short 300 μm foam stems from the incident laser bandwidth (0.9 Å) combined with the diagnostic spectral resolution (0.2 Å) and the laser aperture (0.4 Å). Similar spectra acquired in 7 mg/cc-500 μm foams exhibit larger spectral shifts and widths. In each foam, the spectral shift and width measured at a given scattering angle are the largest at the time when the transmission just starts. Experimental spectra integrated over 200 ps around this time are plotted in Fig. 3(c) for the 300 and 500 μm foams with LSSD. Figure 3(c) clearly evidences that the mean spectral shift increases as the plasma length increases, but it also shows that the spectral width simultaneously increases especially at the largest angle ($\theta_s = 20°$). As the parameters in the 300 and 500 μm foam plasmas (Fig. 1) are very similar in the region $-500\,\mu\text{m} < z < 200\,\mu\text{m}$, the 300 μm foam measurements clearly demonstrate that significant FSBS already occurs in the first half of the 500 μm foam plasma. Then as the laser continues to propagate over a significant remaining plasma length beyond this region in the 500 μm foam case, further FSBS amplification occurs. Thus, the fact that the largest spectral shifts and bandwidths were observed for the largest plasma length is straightforward evidence of the multiple FSBS process. Results recorded in 3 mg/cc-1 mm foam [Fig. 3(d)] show a similarly wide spectrum when the LSSD was not initially applied: As a result of propagation through the plasma, the transmitted light acquired a spectral bandwidth at least twice the one that could be induced on the laser by LSSD [which is also shown in Fig. 3(c)].

Appendix B describes the derivation of the FSBS spatial growth rate of an incoherent laser beam based on the random phase approximation (RPA) [65] and the values of its key parameters (effective spectral widths induced by the optical incoherence, IAW damping rate, and FSBS homogeneous growth rate). Time-resolved measurements indicate that the scattering measured at 12° stops when the FSBS gain computed along the entire plasma has fallen <∼20. This is used to compute the minimum plasma length along which the beam must propagate for significant FSBS develops. In the inhomogeneous plasma profiles shown in Figs. 1(b) and 1(c), the results are given in Fig. 4(a) under the form of the coordinate z_G at which the computed gain reaches 20 as a function of time for the 3 mg/cc-1 mm and 7 mg/cc-500-μm foams without

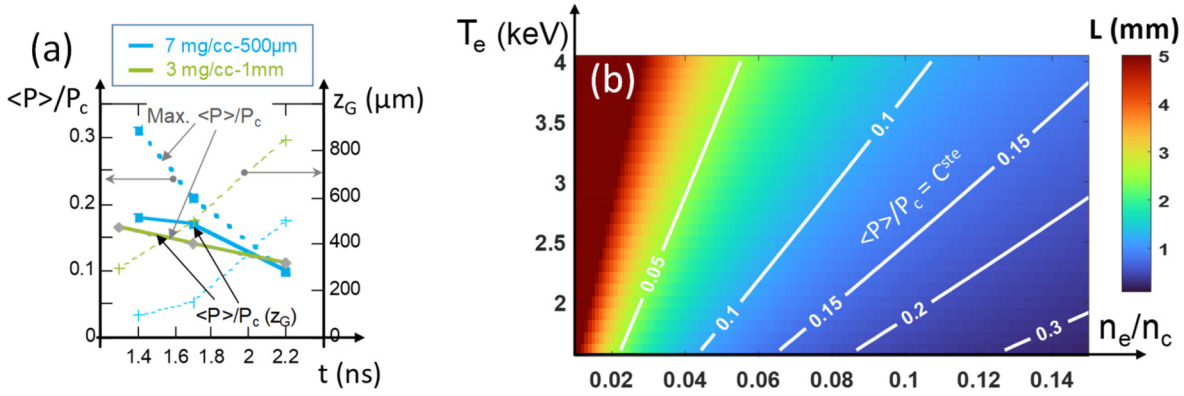

FIG. 4. (a) Time-evolution of the coordinate z_G at which the forward stimulated Brillouin scattering (FSBS) gain computed without longitudinal temporal smoothing by spectral dispersion (LSSD) equals 20, of the value of $\langle P\rangle/P_c$ at z_G and of the maximum of $\langle P\rangle/P_c$ in the entire plasma. (b) Minimum plasma length (L) for the amplification of FSBS up to a computed gain of 20 in a homogeneous low-Z plasma (normalized IAW damping of 0.15) with $Z/A = 0.6$ at given n_e and T_e; the superimposed white curves show the contours of constant $\langle P\rangle/P_c$.

LSSD. At the earliest time ($t = 1.4$ ns), in the 7 mg/cc-500 µm foam plasma, we find $z_G = 100$ µm: This location is ahead of the region where the maximum value of $\langle P\rangle/P_c$ ($\langle P\rangle/P_c \sim 0.3$) was computed using the speckle size fixed by the focusing optics. Figure 4(a) further shows that the maximum $\langle P\rangle/P_c$ experienced by the beam up to z_G is similar in the 3 mg/cc-1 mm and 7 mg/cc-500 µm. This clarifies the fact that similar angular distributions of the scattered light were observed in these two plasmas: After FSBS has developed, it prevails over SF in the remaining plasma. This may simply result from the nonstationary behavior induced on the beam by FSBS [66] and is also consistent with the fact that low-frequency density modulations inhibit SF [67]. This conclusion is reached here in a low-Z plasma in which the IAWs are strongly Landau damped, which minimizes the FSBS amplification, and for the speckles of the megajoule facilities that are among the widest encountered on high-energy facilities. Furthermore, up to $t = \sim 2$ ns, the light scattered in a first FSBS step at $z < z_G$ may still be subject to further FSBS decay steps as it propagates in the regions $z > z_G$, which accounts for the large measured bandwidth [Fig. 3(d)].

While SF can be expected from the plasma entrance provided that intense speckles (with $P_{sp}/P_c > 1$) are present there, FSBS requires a minimum propagation distance before it can give rise to enhanced PII. Figure 4(b) plots this distance as a function of electron density and temperature for a 1.5×10^{15} W/cm^2 LMJ/NIF beamline propagating in a homogeneous plasma. Contours of constant $\langle P\rangle/P_c$ have been superimposed. Figure 4(b) illustrates the expected [31] result that FSBS proceeds over the shortest length in plasmas where $\langle P\rangle/P_c$ is the highest. This simply results from the essentially common functional dependence of $\langle P\rangle/P_c$ and FSBS gain at a fixed IAW damping rate. On the other side, in the highest-temperature plasmas, little SF is expected from the small computed $\langle P\rangle/P_c$, while FSBS amplification could proceed in millimeter plasmas (current ~2 MJ ignition designs [68] involve propagation distances >5 mm, which will keep increasing as these designs are scaled up to even higher laser energies to increase yields). In this paper, we thus demonstrate the need to account for FSBS in the description of the propagation of megajoule beamlines in such ICF plasmas and provide a valuable experimental database to help in this effort.

IV. CONCLUSIONS

The conclusions of this paper open paths of design toward solving critical issues on the road to laser-driven ICF through the angular and spectral broadening [22] that FSBS induces on the laser beams. NIF must currently operate with optical spectral bandwidths between 0.6 and 1.2 Å (at 351 nm) [15,69]. Whereas the latter is likely to increase the detrimental temporal intensity modulations [13] of the pulse and causes a ~13% reduction in the laser energy converted [70] to 3ω, it still remains insufficient for some applications.

The convergence of direct-drive implosions on NIF is indeed presently restrained [71,72] by the laser-irradiation inhomogeneities imprinted on the target early in the laser pulse, with implementation of multiple-frequency optical smoothing [72,73] being considered to go beyond. Instead, FSBS (shown to still develop with LSSD applied) can provide this highest level of irradiation uniformity needed in the first hundreds of picoseconds, while the standard SSD smooths the laser irradiation of the target over the entire laser pulse. The inhibition of SF proves that the plasma does not hydrodynamically follow the nonuniform intensity of the beamline once the latter has experienced FSBS, a clear signature of the ability of PII to control the imprint at the megajoule scale.

At the frontier to ignition, the energy coupled to the target becomes a critical parameter in indirect-drive experiments (a ~10% increase in laser energy recently enabled to cross the ignition threshold [74,75]). The reduced coherence time $\lambda_0^2/(c \times \delta\lambda)$ associated with the increased spectral bandwidth $\delta\lambda$ of a PII beam becomes small enough to reduce backward SBS losses (peak reflectivities >10%) [9,11] developing in the high-Z wall plasma. This is profitable by both increasing the energy coupled to the target and reducing the risks of optics damage [76] without the cost(s) of an increased optically applied spectral width.

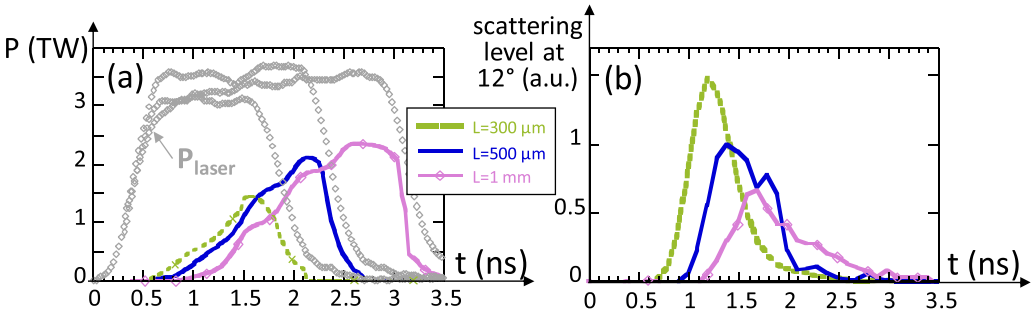

FIG. 5. (a) Laser pulse and power transmitted in the original beam aperture for shots in 7 mg/cc foams with lengths 300 µm, 500 µm, and 1 mm. (b) Corresponding power scattered at $\theta_s = 12°$.

ACKNOWLEDGMENT

The authors acknowledge the operation team of the LIL facility who made this experiment possible.

APPENDIX A: EFFECT OF PLASMA LENGTH MEASURED IN 7 mg/cc FOAMS WITH LSSD

The effect of plasma length was investigated in the LSSD configuration through shots performed in 7 mg/cc foams. Figure 5(a) illustrates the faster complete ionization of shorter foams through their earlier direct transmission. Figure 5(b) shows the increase in instantaneously scattered light levels at 12° as the foam shortens. This observation results from the combination of the time evolution of the transmission of the different plasmas with the efficiency of the mechanisms responsible for the large angle scattering as the plasma parameters evolve. Thus, the larger instantaneous levels measured in shorter foams might result from the higher transmission of the shorter foam plasmas at early times, before the electron density decreases. By contrast, the large angle scattering lasts longer in longer foams because the maximum electron density remains high for longer. These distinct time evolutions eventually result in similar energy scattered at 12° for plasmas of different lengths.

APPENDIX B: DERIVATION OF THE FSBS GROWTH RATE

The RPA equations describe the coupling of the scattered wave with IAWs in the case of an incoherent incident laser wave. They take the following form:

$$(\partial_t + V_{g1z}\partial_z + 2\nu_1)\langle n_1\rangle = 2\gamma_1(\langle n_1\rangle + \langle n_2\rangle),$$
$$(\partial_t + V_{g2z}\partial_z + 2\nu_2)\langle n_2\rangle = 2\gamma_2(\langle n_1\rangle + \langle n_2\rangle),$$

where n_i denotes the spectral density of wave i, with $i = 1$ for the scattered wave and $i = 2$ for the IAW. The coupling constants γ_1 and γ_2 are given by $\gamma_1 \equiv \frac{\gamma_0^2}{\Delta\omega_2}$ and $\gamma_2 \equiv \frac{\gamma_0^2}{\Delta\omega_1}$, $\gamma_0(\sim 10^{12}\ \mathrm{s}^{-1}$ at $\theta_s = 12°$ in this experiment) being the FSBS homogeneous growth rate; ν_2 is the IAW damping rate set by Landau damping in the low-Z foam plasma ($\nu_2 \approx 0.15\, K_2 \times C_s$ [46], $\sim 1.5 \times 10^{11}\ \mathrm{s}^{-1}$ at $\theta_s = 12°$, K_2 being the IAW wave number); ν_1 is the scattered wave damping (and is negligible for our experimental parameters); and V_{g1z} and V_{g2z} denote the projections of the group velocities $\overrightarrow{V_{g1}}$ and $\overrightarrow{V_{g2}}$ along z. The quantities $\Delta\omega_i$ denote the effective spectral widths induced by the laser beam optical incoherence: The larger $\Delta\omega_i$ are, the smaller the coupling constants γ_i become. Here, $\Delta\omega_i$ is given by $\Delta\omega_i = \Delta\omega_{itp} \equiv \mu_i \Delta\omega_{0\mathrm{eff}} + \nu_2$, in the regime where the temporal smoothing is predominant, namely, for $\Delta\omega_{itp} \gg \Delta\omega_{isp}$, and by $\Delta\omega_i = \Delta\omega_{isp} \equiv 1.22 \times \frac{\sigma_i \Delta\theta_0}{2}$ for $\Delta\omega_{isp} \gg \Delta\omega_{itp}$. In these expressions, $\Delta\omega_{0\mathrm{eff}}$ describes the laser temporal incoherence with $\Delta\omega_{0\mathrm{eff}} = \Delta\omega_{0K}/\pi$ when the temporal spectral density $n(\omega_0)$ is a square step function of full width $\Delta\omega_{0K}$; $\Delta\theta_0$ describes the laser spatial incoherence and is half the aperture angle of the quadruplet. The parameters μ_i and σ_i are given by $\mu_1 \equiv |1 - \frac{V_{g1}}{V_{g0}}\cos(\theta_s)|$, $\mu_2 \equiv |1 - \frac{V_{g2}}{V_{g0}}\sin(\frac{\theta_s}{2})| \approx 1$, $\sigma_1 \equiv |V_{g1}K_0 \sin\theta_s| \approx \omega_0 \sin\theta_s$, $\sigma_2 \equiv |V_{g2}K_0|\cos(\theta_s/2) \approx \omega_0 \frac{C_s}{c}$, ω_0 and K_0 being the laser frequency and wave number. Between the two regimes (temporally or spatially predominant), we introduce $A_i \equiv \Delta\omega_{itp}/(1.22\,\sigma_i \Delta\theta_0)$, and interpolate $\Delta\omega_i$ by $\Delta\omega_i = \frac{1.22\sigma_i\Delta\theta_0}{2}[(1 + A_i^2)^{1/2} + A_i]$. The LMJ quadruplet aperture ($\sim f/8$) gives $\Delta\omega_{2sp} \approx 1.9 \times 10^{11}\ \mathrm{s}^{-1}$ at $T_e \sim 2\,\mathrm{keV}$ and $\Delta\omega_2 \approx 2.8 \times 10^{11}\ \mathrm{s}^{-1}$ without LSSD. For the $\Delta\lambda_0 \sim 0.9$ Å spectral bandwidth, $\Delta\omega_{0\mathrm{eff}} = (\omega_0/\pi)(\Delta\lambda_0/\lambda_0) \approx 4 \times 10^{11}\ \mathrm{s}^{-1}$ and $\Delta\omega_2 \approx 6 \times 10^{11}\ \mathrm{s}^{-1}$ in the case with LSSD, so that LSSD corresponds with doubling the IAW effective spectral width obtained in the limit of just a spatial smoothing. Due to the large scattered wave spectral width ($\Delta\omega_{1sp} \approx 4 \times 10^{13}\ \mathrm{s}^{-1}$ for $\theta_s = 12°$) resulting from the spatial smoothing, the effect of the temporal smoothing on $\Delta\omega_1$ is completely negligible resulting in $\Delta\omega_1 = \Delta\omega_{1sp} \approx 4 \times 10^{13}\ \mathrm{s}^{-1}$ with or without LSSD.

The dispersion relation is then readily obtained by replacing ∂_t by 2γ and ∂_z by $2q_{\mathrm{RPA}}$ so that the intensity spatial growth rate $2q_{\mathrm{RPA}}(z)$ may be found by solving the resulting equation $(q_{\mathrm{RPA}}V_{g1z} + \nu_1 - \gamma_1)(q_{\mathrm{RPA}}V_{g2z} + \nu_2 - \gamma_2) = \gamma_1\gamma_2$. Its solution q_{RPA} depends on the parameter $\alpha \equiv (\frac{\Delta\omega_1}{V_{g1z}})/(\frac{\Delta\omega_2}{V_{g2z}})$; one has $\alpha \ll 1$ in the FSBS geometry for the temporal incoherence achievable on laser facilities. In this regime, the solution q_{RPA} as a function of the laser intensity γ_0^2 presents a fast variation around $\gamma_0^2 = \Delta\omega_1\nu_2$. Defining $q_1 \equiv \frac{\gamma_1}{V_{g1z}}$ and $q_2 \equiv (\frac{\gamma_2 - \nu_2}{V_{g2z}})$, q_{RPA} is well approximated by $q_1 = \frac{\gamma_1}{V_{g1z}} = \frac{\gamma_0^2}{\Delta\omega_2 V_{g1z}}$ in the subdomain $\gamma_0^2 \ll \Delta\omega_1\nu_2$ and by q_2 for $\gamma_0^2 \gg \Delta\omega_1\nu_2$, whereas the full RPA dispersion relation has to be solved to get an accurate value of q_{RPA} in the vicinity of $\gamma_0^2 = \Delta\omega_1\nu_2$. We consider that the RPA equations are valid whenever the following usual conditions are

satisfied: (1) $\Delta\omega_1 \gg q_{\mathrm{RPA}} V_{g1z}$, (2) $\Delta\omega_2 \gg q_{\mathrm{RPA}} V_{g2z}$, and (3) $\frac{\gamma_0^2}{(\Delta\omega_1 \Delta\omega_2)} \ll 1$. We now discuss these conditions and the transition to the coherent regime for which the spatial growth rate is $q_{\mathrm{coh}} \equiv \gamma_0^2/(\nu_2 V_{g1z})$ in the strongly damped regime $\gamma_0^2 \ll \nu_2^2(V_{g1z}/V_{g2z})/4$ corresponding to our domain of interest. At any given degree of incoherence, namely, for fixed $\Delta\omega_1$ and $\Delta\omega_2$, the conditions (1)–(3) define a maximum value of γ_0^2 denoted as $\gamma_{0,\mathrm{val}}^2$. It can be checked that, in this domain of validity, the RPA solution $q_{\mathrm{RPA}}(\gamma_0^2)$ remains smaller than or equal to the coherent growth rate $q_{\mathrm{coh}}(\gamma_0^2)$, thus implying the existence of an intermediate domain where none of the incoherent or coherent results apply. An interpolation for the growth rate is therefore needed whenever $q_{\mathrm{RPA}}(\gamma_0^2)$ is smaller than $q_{\mathrm{coh}}(\gamma_0^2)$ at the limit $\gamma_0^2 = \gamma_{0,\mathrm{val}}^2$. For simplicity, we will interpolate the spatial growth rate, denoted as q_{eff}, by keeping the same expression as $q_{\mathrm{RPA}}(\gamma_0^2)$ in this intermediate domain, thus leading to the simple expression $q_{\mathrm{eff}}(\gamma_0^2) = \mathrm{Min}[q_{\mathrm{RPA}}(\gamma_0^2), q_{\mathrm{coh}}(\gamma_0^2)]$ in the whole domain of parameters. In this experiment, as in ICF applications, the strong IAW damping plays a dual role: (i) It pushes the boundary between the RPA regime and the coherent regime [30] toward higher intensities/higher electron densities, and (ii) it leads to a relatively low coherent spatial amplification rate.

In this paper, we focused specifically on $\theta_s = 12^\circ$ for which time and spectrally resolved data were acquired and applied these results to the experiment. As simple metrics of the FSBS strength, we computed the intensity FSBS gain factor G by integrating the intensity spatial growth rate $2q_{\mathrm{eff}}(z)$ along a ray propagating at $\theta_s = 12^\circ$.

[1] S. Atzeni and J. Meyer-ter-Vehn, *The Physics of Inertial Fusion* (Clarendon, Oxford, 2004).

[2] J. D. Lindl, *Inertial Confinement Fusion* (Springer-Verlag, New York, 1998).

[3] Y. Kato, K. Mima, N. Miyanaga, S. Arinaga, Y. Kitagawa, M. Nakatsuka, and C. Yamanaka, Random phasing of high-power lasers for uniform target acceleration and plasma-instability suppression, Phys. Rev. Lett. **53**, 1057 (1984).

[4] S. Skupsky, R. W. Short, T. Kessler, R. S. Craxton, S. Letzring, and J. M. Soures, Improved laser-beam uniformity using the angular dispersion of frequency-modulated light, J. Appl. Phys. **66**, 3456 (1989).

[5] A. Adolf, A. Boscheron, A. Dulac, and E. Journot, Final optic design for the Laser Mégajoule, *Proceedings of SPIE* (SPIE, Monterey, 1999), Vol. 3492, pp. 44–50.

[6] A. N. Mostovych, S. P. Obenschain, J. H. Gardner, J. Grun, K. J. Kearney, C. K. Manka, E. A. McLean, and C. J. Pawley, Brillouin-scattering measurements from plasmas irradiated with spatially and temporally incoherent laser light, Phys. Rev. Lett. **59**, 1193 (1987).

[7] S. H. Glenzer, R. L. Berger, L. M. Divol, R. K. Kirkwood, B. J. MacGowan, J. D. Moody, A. B. Langdon, L. J. Suter, and E. A. Williams, Reduction of stimulated scattering losses from hohlraum plasmas with laser beam smoothing, Phys. Plasmas **8**, 1692 (2001).

[8] Ph. Mounaix, L. Divol, S. Hüller, and V. T. Tikhonchuk, Effects of spatial and temporal smoothing on stimulated Brillouin scattering in the independent-hot-spot model limit, Phys. Rev. Lett. **85**, 4526 (2000).

[9] L. Divol, Controlling stimulated Brillouin backscatter with beam smoothing in weakly damped systems, Phys. Rev. Lett. **99**, 155003 (2007).

[10] M. Duluc, D. Penninckx, P. Loiseau, G. Riazuelo, A. Bourgeade, A. Chatagnier, and E. D'humières, Comparison of longitudinal and transverse smoothing by spectral dispersion on stimulated Brillouin backscattering in inertial confinement fusion plasmas, Phys. Plasmas **26**, 042707 (2019).

[11] R. Berger, C. A. Thomas, K. L. Baker, D. T. Casey, C. S. Goyon, J. Park, N. Lemos, S. F. Khan, M. Hohenberger, J. L. Milovich *et al.*, Stimulated backscatter of laser light from Big-Foot hohlraums on the National Ignition Facility, Phys. Plasmas **26**, 012709 (2019).

[12] H. Wen, R. K. Follett, A. V. Maximov, D. H. Froula, F. S. Tsung, and J. P. Palastro, Suppressing the enhancement of stimulated Raman scattering in inhomogeneous plasmas by tuning the modulation frequency of a broadband laser, Phys. Plasmas **28**, 042109 (2021).

[13] S. Hocquet, D. Penninckx, E. Bordenave, C. Gouédard, and Y. Jaouën, FM-to-AM conversion in high-power lasers, Appl. Opt. **47**, 3338 (2008).

[14] J. H. Kelly, A. Shvydky, J. A. Marozas, M. J. Guardalben, B. E. Kruschwitz, L. J. Waxer, C. Dorrer, E. Hill, A. V. Okishev, and J.-M. Di Nicola, Simulations of the propagation of multiple-FM smoothing by spectral dispersion on OMEGA EP, *Proceedings Volume 8602, High Power Lasers for Fusion Research II* (SPIE, San Francisco, 2013).

[15] K. R. Manes, M. L. Spaeth, J. J. Adams, M. W. Bowers, J. D. Bude, C. W. Carr, A. D. Conder, D. A. Cross, S. G. Demos, J. M. G. Di Nicola *et al.* Damage mechanisms avoided or managed for NIF large optics, Fusion Sci. Technol. **69**, 146 (2016).

[16] J. Néauport, P. Cormont, N. Darbois, A. During, N. Ferriou, E. Lavastre, I. Legoff, D. Leschuitta, C. Maunier, C. Pellegrini *et al.*, Megajoule laser project and polishing processes for high laser induced damage threshold at 351 nm, *Proceedings Volume 5965, Optical Fabrication, Testing, and Metrology II* (SPIE, Jena, 2005).

[17] P. Cormont, C. Houee, B. Da Costa Fernandes, M. Pfiffer, and D. Taroux, Recycle loop deployed for the large optical components of megajoule laser, in *Optical Design and Fabrication 2019 (Freeform, OFT), OSA Technical Digest* (Optica Publishing Group, Washington DC, 2019), paper JT5A.9.

[18] H. A. Rose and D. F. DuBois, Initial development of ponderomotive filaments in plasma from intense hot spots produced by a random phase plate, Phys. Fluids B **5**, 3337 (1993).

[19] D. Pesme, W. Rozmus, V. T. Tikhonchuk, A. Maximov, I. Ourdev, and C. H. Still, Resonant instability of laser filaments in a plasma, Phys. Rev. Lett. **84**, 278 (2000).

[20] V. V. Eliseev, I. Ourdev, W. Rozmus, V. T. Tikhonchuk, C. E. Capjack, and P. E. Young, Ion wave response to intense laser beams in underdense plasmas, Phys. Plasmas **4**, 4333 (1997).

[21] A. J. Schmitt and B. B. Afeyan, Time-dependent filamentation and stimulated Brillouin forward scattering in inertial confinement fusion plasmas, Phys. Plasmas **5**, 503 (1998).

[22] A. V. Maximov, I. G. Ourdev, D. Pesme, W. Rozmus, V. T. Tikhonchuk, and C. E. Capjack, Plasma induced smoothing of a spatially incoherent laser beam and reduction of backward stimulated Brillouin scattering, Phys. Plasmas **8**, 1319 (2001).

[23] R. Y. Chiao, E. Garmire, and C. H. Townes, Self-trapping of optical beams, Phys. Rev. Lett. **13**, 479 (1964).

[24] P. Kaw, G. Schmidt, and T. Wilcox, Filamentation and trapping of electromagnetic radiation in plasmas, Phys. Fluids **16**, 1522 (1973).

[25] C. E. Max, Strong self-focusing due to the ponderomotive force in plasmas, Phys. Fluids **19**, 74 (1976).

[26] L. J. Babati, W. A. Farmer, R. L. Berger, M. A. Belyaev, T. Chapman, D. E. Hinkel, E. Kur, and E. A. Williams, Simulating the filamentation of smoothed laser beams with three-dimensional nonlinear dynamics, AIP Advances **12**, 095005 (2022).

[27] J. Myatt, D. Pesme, S. Hüller, A. Maximov, W. Rozmus, and C. E. Capjack, Nonlinear propagation of a randomized laser beam through an expanding plasma, Phys. Rev. Lett. **87**, 255003 (2001).

[28] P. M. Lushnikov and H. A. Rose, Instability versus equilibrium propagation of a laser beam in plasma, Phys. Rev. Lett. **92**, 255003 (2004).

[29] P. M. Lushnikov and H. A. Rose, How much laser power can propagate through fusion plasma? Plasma Phys. Control. Fusion **48**, 1501 (2006).

[30] M. Grech, G. Riazuelo, D. Pesme, S. Weber, and V. T. Tikhonchuk, Coherent forward stimulated Brillouin scattering of a spatially incoherent laser beam in a plasma and its effect on beam spray, Phys. Rev. Lett. **102**, 155001 (2009).

[31] S. Huller, A. Porzio, and J. Robiche, Order statistics of high-intensity speckles in stimulated Brillouin scattering and plasma-induced laser beam smoothing, New J. Phys. **15**, 025003 (2013).

[32] C. Ruyer, A. Debayle, P. Loiseau, P. E. Masson-Laborde, J. Fuchs, M. Casanova, J. R. Marquès, L. Romagnani, P. Antici, N. Bourgeois *et al.*, Forward scattering and filamentation of a spatially smoothed laser pulse in the hydrodynamic and kinetic frameworks, Phys. Plasmas **28**, 052701 (2021).

[33] M. Grech, V. T. Tikhonchuk, G. Riazuelo, and S. Weber, Plasma induced laser beam smoohing below the filamentation threshold, Phys. Plasmas **13**, 093104 (2006).

[34] J. D. Moody, B. J. MacGowan, S. H. Glenzer, R. K. Kirkwood, W. L. Kruer, A. J. Schmitt, E. A. Williams, and G. F. Stone, First measurement of short length-scale density fluctuations in a large laser plasma, Phys. Rev. Lett. **83**, 1783 (1999).

[35] J. D. Moody, B. J. MacGowan, S. H. Glenzer, R. K. Kirkwood, W. L. Kruer, D. S. Montgomery, A. J. Schmitt, E. A. Williams, and G. F. Stone, Experimental investigation of short scalelength density fluctuations in laser-produced plasmas, Phys. Plasmas **7**, 2114 (2000).

[36] J. Fuchs, C. Labaune, S. Depierreux, H. A. Baldis, A. Michard, and G. James, Experimental evidence of plasma-induced incoherence of an intense laser beam propagating in an underdense plasma, Phys. Rev. Lett. **86**, 432 (2001).

[37] J. Fuchs, C. Labaune, H. Bandulet, P. Michel, S. Depierreux, and H. A. Baldis, Reduction of the coherence time of an intense laser pulse propagating through a plasma, Phys. Rev. Lett. **88**, 195003 (2002).

[38] H. C. Bandulet, C. Labaune, J. Fuchs, P. Michel, J. Myatt, S. Depierreux, and H. A. Baldis, Observation of ion acoustic waves associated with plasma-induced incoherence of laser beams using Thomson scattering, Phys. Rev. E **68**, 056405 (2003).

[39] P. Michel, C. Labaune, H. C. Bandulet, K. Lewis, S. Depierreux, S. Hulin, G. Bonnaud, V. T. Tikhonchuk, S. Weber, G. Riazuelo *et al.*, Strong reduction of the degree of spatial coherence of a laser beam propagating through a preformed plasma, Phys. Rev. Lett. **92**, 175001 (2004).

[40] D. H. Froula, L. Divol, N. B. Meezan, S. Dixit, J. D. Moody, P. Neumayer, B. B. Pollock, J. S. Ross, and S. H. Glenzer, Ideal laser-beam propagation through high-temperature ignition hohlraum plasmas, Phys. Rev. Lett. **98**, 085001 (2007).

[41] D. H. Froula, L. Divol, N. B. Meezan, S. Dixit, P. Neumayer, J. D. Moody, B. B. Pollock, J. S. Ross, L. Suter, and S. H. Glenzer, Laser beam propagation through inertial confinement fusion hohlraum plasmas, Phys. Plasmas **14**, 055705 (2007).

[42] D. Turnbull *et al.*, Beam spray thresholds in ICF-relevant plasmas, Phys. Rev. Lett. **129**, 025001 (2022).

[43] K. Lewis, G. Riazuelo, and C. Labaune, Modeling of imaging diagnostics for laser plasma interaction experiments with the code PARAX, Rev. Sci. Instr. **76**, 093502 (2005).

[44] S. H. Glenzer, D. H. Froula, L. Divol, M. Dorr, R. L. Berger, S. Dixit, B. A. Hammel, C. Haynam, J. A. Hittinger, J. P. Holder *et al.*, Experiments and multiscale simulations of laser propagation through ignition-scale plasmas, Nat. Phys. **3**, 716 (2007).

[45] C. Rousseaux, G. Huser, P. Loiseau, M. Casanova, E. Alozy, B. Villette, R. Wrobel, O. Henry, and D. Raffestin, Laser parametric instability experiments of a 3ω, 15 kJ, 6 ns laser pulse in gas-filled hohlraums at the Ligne d'Intégration Laser facility, Phys. Plasmas **22**, 022706 (2015).

[46] E. A. Williams, R. L. Berger, R. P. Drake, A. M. Rubenchik, B. S. Bauer, D. D. Meyerhofer, A. C. Gaeris, and T. W. Johnston, The frequency and damping of ion acoustic waves in hydrocarbon (CH) and two-ion-species plasmas, Phys. Plasmas **2**, 129 (1995).

[47] D. E. Hinkel, M. D. Rosen, E. A. Williams, A. B. Langdon, C. H. Still, D. A. Callahan, J. D. Moody, P. A. Michel, R. P. J. Town, R. A. London *et al.*, Stimulated Raman scatter analyses of experiments conducted at the National Ignition Facility, Phys. Plasmas **18**, 056312 (2011).

[48] O. S. Jones, C. A. Thomas, P. A. Amendt, G. N. Hall, N. Izumi, M. A. Barrios Garcia, L. F. Berzak Hopkins, H. Chen, E. L. Dewald, D. E. Hinkel *et al.*, Towards a more universal understanding of radiation drive in gas-filled hohlraums, J. Phys. Conf. Ser. **717**, 012026 (2016).

[49] L. Videau, C. Rouyer, J. Garnier, and A. Migus, Motion of hot spots in smoothed beams, J. Opt. Soc. Am. A **16**, 1672 (1999).

[50] F. Walraet, G. Riazuelo, and G. Bonnaud, Propagation in a plasma of a laser beam smoothed by longitudinal spectral dispersion, Phys. Plasmas **10**, 811 (2003).

[51] A. M. Khalenkov, N. G. Borisenko, V. N. Kondrashov, Yu. A. Merkuliev, J. Limpouch, and V. G. Pimenov, Experience of

micro-heterogeneous target fabrication to study energy transport in plasma near critical density, Laser Part. Beams **24**, 283 (2006).

[52] P.-E. Masson-Laborde, S. Depierreux, D. T. Michel, S. Hüller, D. Pesme, J. Robiche, P. Loiseau, V. T. Tikhonchuk, C. Stenz, P. Nicolaï *et al.*, Laser plasma interaction physics on the LIL facility, EPJ Web Conf. **59**, 05003 (2013).

[53] S. Yu Gus'kov, J. Limpouch, Ph. Nicolaï, and V. T. Tikhonchuk, Laser-supported ionization wave in under-dense gases and foams, Phys. Plasmas **18**, 103114 (2011).

[54] K. Nagai, C. S. A. Musgrave, and W. Nazarov, A review of low density porous materials used in laser plasma experiments, Phys. Plasmas **25**, 030501 (2018).

[55] S. Depierreux, C. Labaune, D. T. Michel, C. Stenz, P. Nicolaï, M. Grech, G. Riazuelo, S. Weber, C. Riconda, V. T. Tikhonchuk *et al.*, Laser smoothing and imprint reduction with a foam layer in the multikilojoule regime, Phys. Rev. Lett. **102**, 195005 (2009).

[56] Ph. Nicolaï, M. Olazabal-Loumé, S. Fujioka, A. Sunahara, N. Borisenko, S. Gus'kov, A. Orekov, M. Grech, G. Riazuelo, C. Labaune *et al.*, Experimental evidence of foam homogenization, Phys. Plasmas **19**, 113105 (2012).

[57] C. Goyon, S. Depierreux, V. Yahia, G. Loisel, C. Baccou, C. Courvoisier, N. G. Borisenko, A. Orekhov, O. Rosmej, and C. Labaune, Experimental approach to interaction physics challenges of the shock ignition scheme using short pulse lasers, Phys. Rev. Lett. **111**, 235006 (2013).

[58] S. Depierreux, V. Yahia, C. Goyon, G. Loisel, P.-E. Masson-Laborde, N. Borisenko, A. Orekhov, O. Rosmej, T. Rienecker, and C. Labaune, Laser light triggers increased Raman amplification in the regime of nonlinear Landau damping, Nat. Commun. **5**, 4158 (2014).

[59] V. Yahia, P.-E. Masson-Laborde, S. Depierreux, C. Goyon, G. Loisel, C. Baccou, N. G. Borisenko, A. Orekhov, T. Rienecker, O. Rosmej *et al.*, Reduction of stimulated Brillouin backscattering with plasma beam smoothing, Phys. Plasmas **22**, 042707 (2015).

[60] J. Limpouch, V. T. Tikhonchuk, J. Dostál, R. Dudžák, M. Krupka, N. G. Borisenko, J. Nikl, A. A. Akunets, L. A. Borisenko, and V. G. Pimenov, Characterization of residual inhomogeneities in a plasma created by laser ionization of a low-density foam, Plasma Phys. Controlled Fusion **62**, 035013 (2020).

[61] O. S. Jones, G. E. Kemp, S. H. Langer, B. J. Winjum, R. L. Berger, J. S. Oakdale, M. A. Belyaev, J. Biener, M. M. Biener, D. A. Mariscal *et al.*, Experimental and calculational investigation of laser-heated additive manufactured foams, Phys. Plasmas **28**, 022709 (2021).

[62] M. Cipriani, S. Yu. Gus'kov, F. Consoli, R. De Angelis, A. A. Rupasov, P. Andreoli, G. Cristofari, G. Di Giorgio, and M. Salvadori, Time-dependent measurement of high-power laser light reflection by low-Z foam plasma, High Power Laser Sci. Eng. **9**, e40 (2021).

[63] C. Labaune, S. Depierreux, V. T. Tikhonchuk, D. T. Michel, C. Stenz, N. G. Borisenko, P. H. Nicolaï, S. Hüller, D. Pesme, P. Loiseau *et al.*, Laser-plasma interaction physics in multi kilojoule experiments, J. Phys. Conf. Ser. **244**, 022021 (2010).

[64] E. A. Williams, On the control of filamentation of intense laser beams propagating in underdense plasma, Phys. Plasmas **13**, 056310 (2006).

[65] R. Dautray and J. P. Watteau, *La fusion thermonucléaire inertielle par laser* (CEA, Paris, 1993), Chap. IV.6, pp. 395.

[66] G. Riazuelo and G. Bonnaud, Coherence properties of a smoothed laser beam in a hot plasma, Phys. Plasmas **7**, 3841 (2000).

[67] W. L. Kruer, Interaction physics for megajoule laser fusion targets, in *Laser Interaction and Related Plasma Phenomena*, edited by G. H. Miley and H. Hora (Springer, Boston, 1992), Vol. 10, pp. 503–509.

[68] A. L. Kritcher, A. B. Zylstra, D. A. Callahan, O. A. Hurricane, C. R. Weber, D. S. Clark, C. V. Young, J. E. Ralph, D. T. Casey, A. Pak *et al.*, Design of an inertial fusion experiment exceeding the Lawson criterion for ignition, Phys. Rev. E **106**, 025201 (2022).

[69] M. L. Spaeth, K. R. Manes, D. H. Kalantar, P. E. Miller, J. E. Heebner, E. S. Bliss, D. R. Spec, T. G. Parham, P. K. Whitman, P. J. Wegner *et al.*, Description of the NIF Laser, Fusion Sci. Technol. **69**, 25 (2016).

[70] J. E. Rothenberg, B. Moran, P. Wegner, and T. Weiland, Performance of smoothing by spectral dispersion (SSD) with frequency conversion on the beamlet laser for the National Ignition Facility, Technical Digest, Summaries of Papers Presented at the Conference on Lasers and Electro-Optics (IEEE, San Francisco, 1998), Vol. 6, pp. 344–345.

[71] P. B. Radha, M. Hohenberger, D. H. Edgell, J. A. Marozas, F. J. Marshall, D. T. Michel, M. J. Rosenberg, W. Seka, A. Shvydky, T. R. Boehly *et al.*, Direct drive: Simulations and results from the National Ignition Facility, Phys. Plasmas **23**, 056305 (2016).

[72] T. J. B. Collins, J. A. Marozas, K. S. Anderson, R. Betti, R. S. Craxton, J. A. Delettrez, V. N. Goncharov, D. R. Harding, F. J. Marshall, R. L. McCrory *et al.*, A polar-drive–ignition design for the National Ignition Facility, Phys. Plasmas **19**, 056308 (2012).

[73] J. E. Rothenberg, Comparison of beam-smoothing methods for direct-drive inertial confinement fusion, J. Opt. Soc. Am. B **14**, 1664 (1997).

[74] M. Schirber, Gaining ground in nuclear fusion, Physics **15**, 195 (2022).

[75] M. Zepf, Fusion turns up the heat, Physics **15**, 67 (2022).

[76] T. Chapman, P. Michel, J.-M. G. Di Nicola, R. L. Berger, P. K. Whitman, J. D. Moody, K. R. Manes, M. L. Spaeth, M. A. Belyaev, C. A. Thomas *et al.*, Investigation and modeling of optics damage in high-power laser systems caused by light backscattered in plasma at the target, J. Appl. Phys. **125**, 033101 (2019).